Simulation of sound fields using realistic boundary conditions

Jochen Metzger and Manfred Kaltenbacher
TU Wien, 1060 Wien, Austria, Email: jochen.metzger@tuwien.ac.at

Introduction

For a precise simulation of sound fields the wave equation has to be solved with realistic boundary conditions (BCs). Therefore, the knowledge and description of the acoustic boundaries plays a key role in the calculation of acoustic fields.

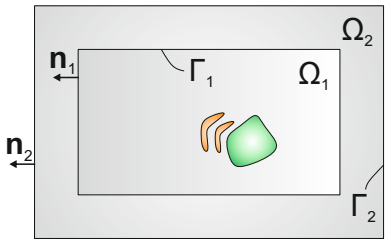

Figure 1: Computational setup consisting of two domains Ω_1 and Ω_2.

In fig. 1 a setup is shown containing two domains Ω_1 and Ω_2, whereas the interface between both domains is Γ_1. This can be a typical setup for a room (Ω_1) surrounded by acoustic absorbers (Ω_2). The weak form of the partial differential equation (PDE) in the frequency domain reads as

$$\int\limits_{\Omega_1\cup\Omega_2} \varphi k^2 P_\mathrm{a}\mathrm{d}\Omega - \int\limits_{\Omega_1\cup\Omega_2} \nabla\varphi\cdot\nabla P_\mathrm{a}\mathrm{d}\Omega + \int\limits_{\Gamma_2} \varphi\frac{\partial P_\mathrm{a}}{\partial \mathbf{n}_2}\mathrm{d}\Gamma = 0\,. \tag{1}$$

In (1) P_a is the acoustic pressure, φ is a test function, k is the wavenumber, Γ_2 is the surface of Ω_2, $\mathbf{n}_2$ the unit normal vector of the surface Γ_2 and $\Omega_1\cup\Omega_2$ is the overall simulation domain. Now, we assume that we can model the absorption behavior in Ω_2 by a boundary condition on Γ_1. Thereby, the PDE reduces to

$$\int\limits_{\Omega_1} \varphi k^2 P_\mathrm{a}\mathrm{d}\Omega - \int\limits_{\Omega_1} \nabla\varphi\cdot\nabla P_\mathrm{a}\mathrm{d}\Omega + \int\limits_{\Gamma_1} \varphi M(P_\mathrm{a})\mathrm{d}\Gamma = 0\,. \tag{2}$$

Here, $M(P_\mathrm{a}) = \frac{\partial P_\mathrm{a}}{\mathbf{n}_1}$ denotes a general boundary operator. As a first order approximation of this operator, the acoustic surface impedance (also known as wall impedance) Z_W at perpendicular sound incidence is used conventionally. In this case, (2) reads as

$$\int\limits_{\Omega_1} \varphi k^2 P_\mathrm{a}\mathrm{d}\Omega - \int\limits_{\Omega_1} \nabla\varphi\cdot\nabla P_\mathrm{a}\mathrm{d}\Omega - \int\limits_{\Gamma_1} \varphi j\omega\rho_0\frac{P_\mathrm{a}}{Z_\mathrm{W}}\mathrm{d}\Gamma = 0\,, \tag{3}$$

where ω is the angular frequency, j the complex unit and ρ_0 is the density of the propagation medium in Ω_1. The acoustic surface impedance at an interface can be determined at perpendicular sound incidence by means of an impedance tube [1] or at oblique angles of incidence [2], e.g. employing a subtraction technique in time domain [3] or a spatial Fourier transform method in the wave number domain [4]. The acoustic surface impedance at perpendicular sound incidence only models locally reacting interfaces, where the acoustic impedance is not a function of the angle of sound incidence. To model interfaces which are non–locally reacting, the acoustic impedance has to depend on the angle of sound incidence. This circumstance necessitates an operator M of higher order along with an increased calculation effort. In contrast, we also model the domain Ω_2 (absorber) using effective material parameters and solve for a wave equation for inhomogeneous fluids. The method is described and a validation by means of comparison with analytic calculations and measurement results is done.

Helmholtz equation for inhomogeneous fluids

We assume an isentropic state in a non–viscous, stagnant fluid. Furthermore, we consider a perturbation ansatz according to

$$p = p_0 + p_\mathrm{a};\quad \rho = \rho_0 + \rho_\mathrm{a};\quad \mathbf{v} = \mathbf{v}_\mathrm{a}\,, \tag{4}$$

with the properties $p_\mathrm{a} \ll p_0$ and $\rho_\mathrm{a} \ll \rho_0$. In this pertubation ansatz, p is the pressure, p_a the acoustic pressure, ρ the density, ρ_a the acoustic density and $\mathbf{v}_\mathrm{a}$ the acoustic particle velocity. The mean quantities are denoted with index 0. By inserting the perturbation ansatz into the conservation of mass and momentum [5], the linearized conservation equations read as

$$\frac{\partial\rho_\mathrm{a}}{\partial t} + \nabla\cdot(\rho_0\mathbf{v}_\mathrm{a}) = q_\mathrm{ma} \tag{5}$$

$$\rho_0\frac{\partial\mathbf{v}_\mathrm{a}}{\partial t} + \nabla p_\mathrm{a} = \mathbf{q}_\mathrm{mo}\,, \tag{6}$$

where q_ma and $\mathbf{q}_\mathrm{mo}$ model source terms. The mass conservation (5) inserted in the linearized pressure–density relation

$$\frac{\partial p_\mathrm{a}}{\partial t} = c_0^2\left(\frac{\partial\rho_\mathrm{a}}{\partial t} + \mathbf{v}_\mathrm{a}\cdot\nabla\rho_0\right) \tag{7}$$

and a rearrangement of (6) provides

$$\frac{1}{\rho_0 c_0^2}\frac{\partial p_\mathrm{a}}{\partial t} + \nabla\cdot\mathbf{v}_\mathrm{a} = \frac{1}{\rho_0}q_\mathrm{ma} \tag{8}$$

$$\frac{\partial\mathbf{v}_\mathrm{a}}{\partial t} + \frac{1}{\rho_0}\nabla p_\mathrm{a} = \frac{1}{\rho_0}\mathbf{q}_\mathrm{mo}\,. \tag{9}$$

In (7) and (8), c_0 is the speed of sound. Applying a time derivative to (8) and a spatial derivative to (9), Fourier transform and subtracting both equations, the Helmholtz equation for inhomogeneous fluids can be derived with

$$\frac{\omega^2}{K_\mathrm{s}} P_\mathrm{a} + \nabla \cdot \frac{1}{\rho_0} \nabla P_\mathrm{a} = \nabla \cdot \frac{\mathbf{Q}_\mathrm{mo}}{\rho_0} - j\omega \frac{Q_\mathrm{ma}}{\rho_0} \,. \tag{10}$$

In (10), $K_\mathrm{s} = \rho_0 c_0^2$ is the bulk modulus, whereas $\mathbf{Q}_\mathrm{mo}$ and Q_a are the time Fourier transformed source terms introduced in (5) and (6). By applying the chain rule, we arrive at

$$\frac{\omega^2}{K_\mathrm{s}} P_\mathrm{a} + \nabla \cdot \nabla P_\mathrm{a} - \frac{1}{\rho_0^2} \nabla \rho_0 \cdot \nabla P_\mathrm{a} = \nabla \cdot \frac{\mathbf{Q}_\mathrm{mo}}{\rho_0} - j\omega \frac{Q_\mathrm{ma}}{\rho_0} \,. \tag{11}$$

In (11), the influence of a space dependent density ρ_0 is described by the third term, which is equal to zero in an homogeneous fluid.

Validation of the method

To validate the method, the acoustic pressure is calculated by solving (11) by means of our in house Finite–Element (FE) software CFS++[5]. We compare this acoustic pressure to the one obtained by means of analytic calculating the acoustic pressure field in front of an absorber – air interface using the spatial Fourier transform method. Moreover, the results are compared with measurement ones.

Simulation setup for FE–simulation

The axisymmetric simulation setup for the validation of the method can be seen in fig. 2. The setup consists of two domains Ω_1 and Ω_2 with the material parameters density ρ_{0i} and bulk modulus $K_{\mathrm{s}i}$ ($i = \{1, 2\}$). Both domains are surrounded with a perfectly matched layer (PML) for modeling free radiation. Furthermore, the bottom of Ω_2 is totally reflecting (sound hard). The sound source in the validation setup is placed 100 mm above the interface. The acoustic pressure is investigated at an observer point between the sound source and interface and at an observer line 20 mm in front of the interface.

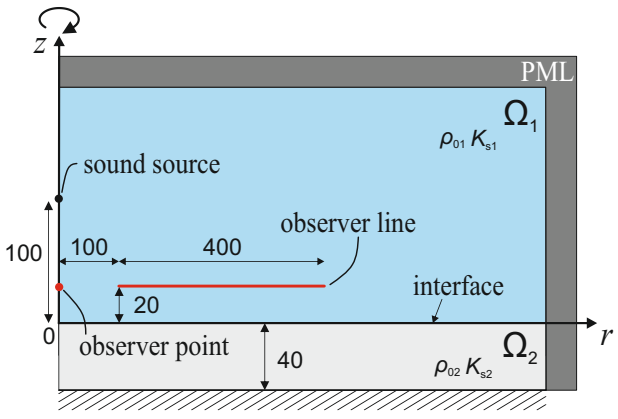

Figure 2: Setup for validation.

Analytic calculation of the acoustic field

We assume a plane z = const. with an axisymmetric spatial distribution of the acoustic pressure P_a. Hence, the acoustic pressure $P_\mathrm{a}(r)$ only depends on the radius r. The spatial Fourier transform (denoted with $\sim$) of the acoustic pressure computes by [6]

$$\tilde{P}_\mathrm{a}(k_r) = 2\pi \int_0^\infty P_\mathrm{a}(r) J_0(r k_r) r \mathrm{d}r \,. \tag{12}$$

In (12), J_0 is the Bessel function of first kind and 0th order and k_r the radial component of the wave vector. The wave vector is given by

$$\mathbf{k} = \begin{pmatrix} k_r \\ k_z \end{pmatrix} = \begin{pmatrix} k \sin\theta_\mathrm{i} \\ k \cos\theta_\mathrm{i} \end{pmatrix} \,, \tag{13}$$

with the angle of sound incidence (angle between $\mathbf{k}$ and the z–axis) θ_i. The inverse Fourier transform of the acoustic pressure is defined as

$$P_\mathrm{a}(r) = \frac{1}{2\pi} \int_0^\infty \tilde{P}_\mathrm{a}(k_r) J_0(r k_r) k_r \mathrm{d}k_r \,. \tag{14}$$

The inverse Fourier transform can be interpreted in such a way that the acoustic pressure distribution on a plane can be represented by a sum of an infinite number of harmonic components. Any kind of wave can therefore be decomposed in a set of plane waves by using the spatial Fourier transform [7]. We assume a setup which is shown in fig. 2 with a sound source located at the z–axis and a sound reflecting surface at $z = 0$. In difference to the setup shown in fig. 2, the interface between both domains is infinite in the analytic computation of the acoustic pressure. The acoustic pressure between the interface and the sound source (placed at z_s) for $0 \leq z \leq z_\mathrm{s}$ can be decomposed into an incident $P_\mathrm{a,i}$ and reflected part $P_\mathrm{a,r}$

$$P_\mathrm{a}(r, z) = P_\mathrm{a,i}(r, z) + P_\mathrm{a,r}(r, z) \,. \tag{15}$$

The incident part can be described with the acoustic pressure caused by the sound source spreading into a free field. The reflected part can be calculated by using the inverse spatial Fourier transform defined in (14), whereas the spatial Fourier transformed reflected acoustic pressure can be replaced by P_i and R (being the sound pressure reflection coefficient of the interface). Thus, the acoustic pressure can be calculated by [8]

$$P_\mathrm{a,r}(r, z) = P_\mathrm{i} + \frac{1}{2\pi} \int_0^\infty \tilde{P}_\mathrm{i}(z_\mathrm{s}) R e^{-j k_z (z_\mathrm{s} + z)} J_0(r k_r) k_r \mathrm{d}k_r \,. \tag{16}$$

For the calculation of (16), the spatial Fourier transformed acoustic pressure of the incoming acoustic pressure (free field radiation) is needed. Furthermore, an approximation of the integral in (16) is done by using the adaptive Gauß-Kronrod quadrature.

Measurement setup

To measure the sound field above a rockwool sample with thickness 40 mm, a BK 4187 1/4" microphone is mounted on a 2D–gantry by means of a tube. The gantry allows to scan the sound field above the sample in a range of 195 cm x 20 cm. The sound source we used for measurements is built of two Visaton BF45 in a spherical containment made of wood. The resulting sound source shows a dipole like polar pattern. In the measurements, the axis of the sound source is arranged perpendicular to the surface of the planar sample. The measurement setup for the validation is displayed in fig. 3. Here, the 2D–gantry with the tube to place the microphone between the rockwool sample and the loudspeaker can be seen. Since the measurements are performed in an ordinary room, the evaluation of the recorded acoustic pressure is done by means of calculating the impulse response, similar to the procedure described in [3]. In the measurement setup, the nearest sound reflecting objects are located more than 1 m away. Thus, the parts of the impulse response, which are caused by reflections can be expected at 6 ms. The excitation signal is a maximum length sequence (MLS) with length 10 s with 50,000 samples/s.

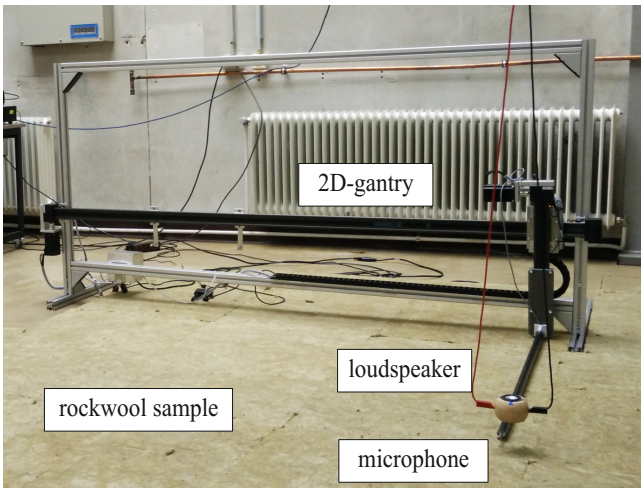

Figure 3: Measurement setup for validation.

Validation results

In the first validation example, both domains are modeled with the same material parameters of air ($\rho_{0i} = 1.2\,\mathrm{kg/m^3}$, $K_{si} = 138720\,\mathrm{Pa}$, $i = \{1, 2\}$).

In fig. 4 the acoustic sound pressure level (SPL) at the observer point is shown as a function of frequency. Here, the analytical results using (16) with a time Fourier transformed acoustic pressure [9] and the spatial Fourier transformed acoustic pressure of a dipole with free radiation [8] is shown in solid blue. In the FE–simulations (shown in solid orange), the dipole is modeled by means of two monopoles with same strengths but different sign. The analytic dipole formula models an ideal dipole, where two monopoles are placed at an infinite small distance. Therefore, the analytic calculations using (16) (shown as dashed orange line) are also performed by using two monopoles placed with a distance of 1 mm to each other.

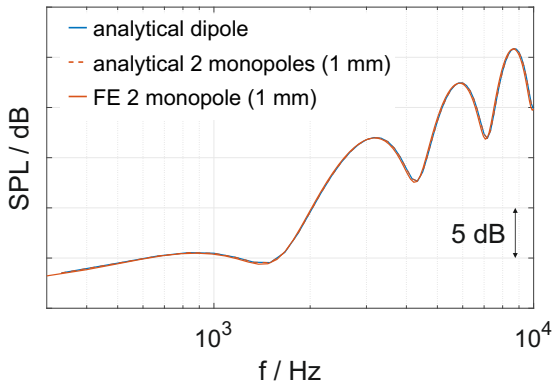

Figure 4: SPL as a function of excitation frequency (Ω_1: air, Ω_2: air).

The same distance between the monopoles is used as in the FE–simulations. It can be seen that the SPL at the observer increases with higher frequencies. There is nearly no difference between the three calculation methods of the acoustic pressure at the observer. This allows the approximation of the ideal dipole by means of two monopoles with a distance of 1 mm. This setup of the sound source is used in the following calculations.

Now, we investigate a sound field above an absorber. In doing so, domain Ω_1 is modeled as air and domain Ω_2 is modeled as an isotropic sound absorbing fluid. The material parameters are calculated by applying the Komatsu–model [10] with a flow resistance of $9.5\,\mathrm{kPas/m^2}$. With this model, the characteristic field impedance Z_C and the wave number k_C can be computed. The effective material parameter for Ω_2 are obtained by

$$K_{s2} = Z_\mathrm{C}\frac{\omega}{k_\mathrm{C}}; \quad \rho_{02} = Z_\mathrm{C}\frac{k_\mathrm{C}}{\omega}. \tag{17}$$

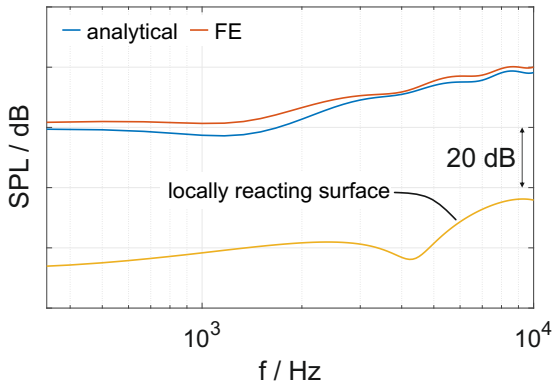

Figure 5: SPL as a function of excitation frequency (Ω_1: air, Ω_2: absorber).

In fig. 5 the SPL at the observer point above the absorber is displayed. In this case, similar to the previous validation example, an increasing SPL with higher frequencies can be observed. Furthermore, the SPL at the observer point computed by solving (3) with the FE method using the acoustic surface impedance at perpendicular sound incidence is shown. The results are compared with the analytic solution of the acoustic pressure and the acoustic

pressure obtained by solving (11) with the FE method. It can be seen that the modeling of the interface with a locally reacting surface gives no sufficient agreement to the analytic solution. The acoustic pressure is underestimated with more than 40 dB at all frequencies between 300 Hz and 10 kHz. The sound reflecting interface in the analytic calculations is infinite, whereas the absorber has finite dimensions in the FE calculations. Probably this can cause the deviations, which can be found between the analytic and FE calculations.

In fig. 6, the acoustic pressure in terms of the real part along the observer line can be seen for an exemplary frequency of 5 kHz. It can be seen that the displayed segment of the sound field shows approximately 5 periods with a wavelength of 6.86 cm along the observer line. It can be stated, that the FE calculations show good agreement to the analytic calculations. The measurement results on the other hand, show a slightly larger acoustic wavelength in comparison to both results of the calculations. Due to the spatial averaging of the microphone (the membrane is not infinitesimal) these deviations can be explained. However, the obtained acoustic pressure by solving (11) shows good agreement especially in comparison to the analytic solution.

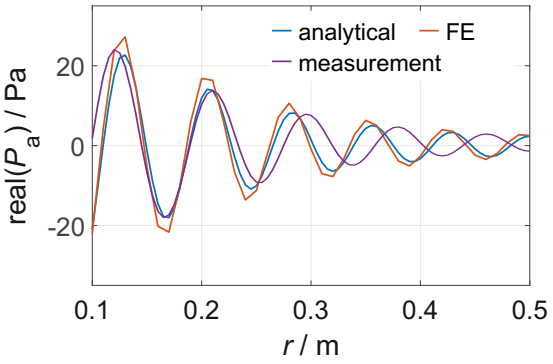

Figure 6: Real part of the acoustic pressure as a function of space at 5 kHz (Ω_1: air, Ω_2: absorber).

Conclusion and outlook

In this paper, we presented a method for the calculation of acoustic fields. In this method, the influence of a layer of absorber material is not modeled by means of the acoustic surface impedance but by an isotropic absorbing fluid. The method is explained and the PDE for inhomogeneous fluids is derived. Furthermore, the validation of the method is presented in terms of a comparison with the analytic calculation of the acoustic pressure at an observer point and at an observer line. The comparison to the analytic calculation and to the measurement of the observed acoustic pressure show good agreement.

In future, measurement results of the acoustic surface impedance by means of a spatial Fourier transform method (similar to the one presented in [4]) will be used for the calculation of the material parameters of the absorber domain. This allows for further investigations of the method presented in this paper at a real absorber – interface.

References

[1] ISO 10534-2: Acoustics - Determination of sound absorption coefficient and impedance in impedance tubes - Part 2: Transfer-function method, 1998.

[2] Metzger, J. and Kaltenbacher, M.: A comparison of measurement techniques to determine the acoustic impedance at oblique sound incidence angle. In: Proceedings of DAGA 2015 - 41st German Annual Conference on Acoustics, Nuremberg, Germany, 2015, 780–783.

[3] Metzger, J., Tschallener, S. and Kaltenbacher, M.: Separation of an incoming and reflecting impulse for determining angle-dependent acoustic properties in situ. In: Proceedings of DAGA 2016 - 42nd German Annual Conference on Acoustics, Aachen, Germany, 2016, 802–805.

[4] Tamura, M.: Spatial Fourier transform method of measuring the reflection coefficient at oblique incidence. I: Theory and numerical examples. The Journal of Acoustical Society of America 88(5), 1990, 2259–2264.

[5] Kaltenbacher, M.: Numerical Simulation of Mechatronic Sensors and Actuators: Finite–Elements for computational multiphysics. Springer, Berlin, 2015.

[6] Williams, E. G.: Fourier Acoustics: Sound Radiation and Nearfield Acoustical Holography, Academic Press, 1999.

[7] Maynard, J.D., Williams, E.G., and Lee, Y.: Nearfield acoustic holography: I. Theory of generalized holography and the development of NAH. The Journal of Acoustical Society of America 78(4), 1985, 1395–1413.

[8] Morse, P. M., and Ingard, K. U.: Theoretical Acoustics. McGraw Hill Book Company, 1968.

[9] Kuttruff, H.: Acoustics: An Introduction. Taylor & Francis, London & New York, 2007.

[10] Komatsu, T.: Improvement of the Delany–Bazley and Miki models for fibrous sound–absorbing materials. Acoustical science and technology 29(2), 2008, 121–129.